A blueprint for detecting supersymmetric dark matter in the Galactic halo

V. Springel[1], S. D. M. White[1], C. S. Frenk[2], J. F. Navarro[3,4], A. Jenkins[2], M. Vogelsberger[1], J. Wang[1], A. Ludlow[3], A. Helmi[5]

[1]*Max-Planck-Institute for Astrophysics, Karl-Schwarzschild-Str. 1, 85740 Garching, Germany*

[2]*Institute for Computational Cosmology, Dep. of Physics, Univ. of Durham, South Road, Durham DH1 3LE, UK*

[3]*Dep. of Physics & Astron., University of Victoria, Victoria, BC, V8P 5C2, Canada*

[4]*Department of Astronomy, University of Massachusetts, Amherst, MA 01003-9305, USA*

[5]*Kapteyn Astronomical Institute, Univ. of Groningen, P.O. Box 800, 9700 AV Groningen, The Netherlands*

Dark matter is the dominant form of matter in the universe, but its nature is unknown. It is plausibly an elementary particle, perhaps the lightest supersymmetric partner of known particle species[1]. In this case, annihilation of dark matter in the halo of the Milky Way should produce γ-rays at a level which may soon be observable[2,3]. Previous work has argued that the annihilation signal will be dominated by emission from very small clumps[4,5] (perhaps smaller even than the Earth) which would be most easily detected where they cluster together in the dark matter halos of dwarf satellite galaxies[6]. Here we show, using the largest ever simulation of the formation of a galactic halo, that such small-scale structure will, in fact, have a negligible impact on dark matter detectability. Rather, the dominant and likely most easily detectable signal will be produced by diffuse dark matter in the main halo of the Milky Way[7,8]. If the main halo is strongly detected, then small dark matter clumps should also be visible, but may well contain no stars, thereby confirming a key prediction of the Cold Dark Matter (CDM) model.

If small-scale clumping and spatial variations in the background are neglected, then it is easy to show that the main halo would be much more easily detected than the halos of known satellite galaxies. For a smooth halo of given radial profile shape, for example NFW[9], the annihilation luminosity can be written as $L \propto V_{\rm max}^4/r_{\rm half}$, where $V_{\rm max}$ is the maximum of the circular velocity curve and $r_{\rm half}$ is the radius containing half the annihilation flux. (For an NFW profile $r_{\rm half} = 0.089\, r_{\rm max}$, where $r_{\rm max}$ is the radius at which the circular velocity curve peaks.) The flux from an object at distance d therefore scales as $V_{\rm max}^4/(r_{\rm half}\, d^2)$, while the angular size of the emitting region scales as $r_{\rm half}/d$. Hence, the signal-to-noise for detection against a bright uniform background scales as $S/N \propto C V_{\rm max}^4/(r_{\rm half}^2\, d)$. The constant C depends only weakly on profile shape (see Supplementary Information). For the CDM simulation of the Milky Way's halo we present below, $V_{\rm max} \simeq 209\,{\rm km\,s^{-1}}$, $r_{\rm max} \simeq 28.4\,{\rm kpc}$ and $d \simeq 8\,{\rm kpc}$. Using parameters for Milky Way satellite halos from previous modelling[10,11], the highest S/N is predicted for the Large Magellanic Cloud (LMC), for which $V_{\rm max} \simeq 65\,{\rm km\,s^{-1}}$, $r_{\rm max} \simeq 13\,{\rm kpc}$ and $d = 48\,{\rm kpc}$, leading to $(S/N)_{\rm MW}/(S/N)_{\rm LMC} = 134$! (Note that this overestimates the contrast achievable in practice; see Supplementary Information.)

The simulations used in this Letter are part of the Virgo Consortium's Aquarius Project[12] to simulate the formation of CDM halos similar to that of the Milky Way. The largest simulation has a dark matter particle mass of 1712 $\rm M_\odot$ and a converged length scale of 120 pc, both of which improve by a factor of 3 over the largest previous simulation[13]. This particular halo has mass $M_{200} = 1.84 \times 10^{12}\,{\rm M_\odot}$ within $r_{200} = 246\,{\rm kpc}$, the radius enclosing a mean density 200 times the critical value. Simulations of the *same* object at mass resolutions lower by factors of 8, 28.68, 229.4 and 1835 enable us to check explicitly for the convergence of the various numerical quantities presented below.

The detectable annihilation luminosity density at each point within a simulation is

$$\mathscr{L}(\mathbf{x}) = \mathscr{G}(\text{particle physics}, \text{observational setup})\,\rho^2(\mathbf{x}),$$

where the constant $\mathscr{G}$ does not depend on the structure of the system but encapsulates the properties of the dark matter particle (e.g. annihilation cross-section and branching ratio into photons) as well as those of the telescope and observation. For the purposes of this Letter, we set $\mathscr{G} = 1$ and give results only for the relative luminosities and detectability of the different structures. In this way, we can quote results that are independent of the particle physics model and the observational details.

Figure 1 shows the distribution of annihilation radiation within our Milky Way halo as a function of the resolution used to simulate it. This plot excludes the contribution to the emission from resolved substructures. Half of the emission from the Milky Way halo is predicted to come from within 2.57 kpc and 95% from within 27.3 kpc. For the lowest resolution simulation (1835 times coarser than the largest simulation), the luminosity is clearly depressed below 3 kpc, but for the second best simulation, it converges well for $r > 300$ pc. Thus we infer that the largest simulation should give convergent results to $r \sim 150$ pc, and that numerical resolution affects the luminosity of the main diffuse halo only at the few percent level. Note that much larger effects will be caused by the baryonic component of the Milky Way, which we neglect. This is expected to compress the inner dark matter distribution and thus to enhance its annihilation signal[14], which would strengthen our conclusions. (See the Supplementary Information for discussion of this and related topics.)

Within 433 kpc of the halo centre, we identify 297,791 and 45,024 self-bound subhalos in our two highest resolution simulations. Many of these can be matched individually in the two simulations, allowing a crucial (and never previously attempted) test of the convergence of

their internal structure. In Fig. 2 we show the results of such a test. The values inferred for $V_{\rm max}$ show no systematic offsets between simulation pairs down to the smallest objects detected in the lower resolution simulation, suggesting that $V_{\rm max}$ values are reliable above $\sim 1.5\,{\rm km\,s^{-1}}$ in the largest simulation. Systematic offsets are visible in each simulation at small $r_{\rm max}$, reaching 10% on a scale which decreases systematically as the resolution increases. From this, we conclude that our largest simulation produces $r_{\rm max}$ values which are accurate to 10% for $r_{\rm max} > 165\,{\rm pc}$. Figure 1 shows that almost all the annihilation signal from a halo comes from $r \ll r_{\rm max}$, corresponding to scales which are not well resolved for most subhalos. In the following we will therefore assume the annihilation luminosity from the diffuse component of each subhalo to be $L = 1.23\mathscr{G}V_{\rm max}^4/{\rm G}^2 r_{\rm max}$, the value expected for an object with NFW structure.

When estimating the Milky Way's annihilation luminosity from our simulations, we need to include the following components: (1) smooth emission associated with the main halo (hereafter, MainSm); (2) smooth emission associated with resolved subhalos (SubSm); (3) emission associated with unresolved substructure in the main halo (MainUn); and (4) emission associated with substructure within the subhalos themselves (SubSub). (Here we do not discuss emission from dark matter caustics[15].) These 4 components have very different radial distributions both within the Milky Way and within its substructures. Neglect of this crucial fact in previous work (see below) has led to incorrect assessments of the importance of small-scale substructure for the detectability of the annihilation radiation.

The solid blue line in Fig. 3 shows $M(<r)/M_{200}$, where $M(<r)$ is the mass within r. Half of M_{200} lies within 98.5 kpc and only 3.3% within the Solar circle ($r = 8\,{\rm kpc}$). The solid red line shows the corresponding curve for the MainSm annihilation luminosity, normalized by L_{200}, its value at r_{200}. This component is much more centrally concentrated than the mass; its half-luminosity radius is only 2.62 kpc. In contrast, the thick green line shows that the SubSm

luminosity is much *less* centrally concentrated than the mass. This is a result of the dynamical disruption of substructure in the inner regions of the halo. The thick green line includes contributions from all substructures with mass exceeding $10^5\,\mathrm{M}_\odot$, almost all of which have converged values for $V_{\rm max}$ and $r_{\rm max}$. This line is also normalized by L_{200}. Within r_{200}, SubSm contributes 76% as much luminosity as MainSm, but within 30 kpc, for example, this fraction is only 2.5%.

The three thin green lines in Fig. 3 show the results of excluding contributions from less massive subhalos, corresponding to thresholds, $M_{\rm thr} = 10^6, 10^7$ and $10^8\mathrm{M}_\odot$. These all have similar shape and are offset approximately equally in amplitude, implying that SubSm luminosity scales as $M_{\rm thr}^{-0.226}$ at all radii. If we assume, in the absence of other information, that this behaviour continues down to a minimum mass of $10^{-6}\,\mathrm{M}_\odot$, which might be appropriate if the dark matter is the lightest supersymmetric particle[16], then the MainUn and SubSm have the same radial distribution. We predict these two components together to be 232 times more luminous than MainSm within r_{200}, but still only 7.8 times more luminous within 30 kpc. A distant observer would thus infer the substructure population of the Milky Way to be 232 times brighter than its smooth dark halo, but from the Earth's position the total boost is predicted to be only 1.9 since the substructure signal typically comes from much larger distances.

We must now consider the additional luminosity due to (sub-)substructures (SubSub). Before a subhalo is accreted onto the main object, we assume its detailed structure to be similar to that of the main halo (including its subhalo population), but scaled down appropriately in mass and radius. (We have checked that such a scaling does indeed hold approximately for small independent objects outside the main halo.) However, once the subhalo is accreted, its outer regions are rapidly removed by tidal stripping. The longer a subhalo has been part of the main system and the closer it is to the centre, the more drastic is the stripping[17,18]. As a result,

most of the substructure associated with the subhalo is removed, while its smooth luminosity is little affected. The removed (sub-)subhalos are, in effect, transferred to components SubSm and MainUn.

A subhalo at Galactocentric distance r is typically truncated at tidal radius $r_t = (M_{\rm sub}/[(2-{\rm dln}M/{\rm dln}r)\,M(<r)])^{1/3}r$. We estimate its SubSub luminosity by assuming that all material beyond r_t is simply removed. The remaining SubSub luminosity can then be obtained from the curves of Fig. 3 if we scale them to match the measured parameters of the subhalo ($M_{\rm sub}$, $V_{\rm max}$ and $r_{\rm max}$). We assume that the r_{200} of the subhalo before accretion was proportional to its present $V_{\rm max}$. (r_{200} is indeed nearly proportional to $V_{\rm max}$ for isolated halos in our simulations.) We further assume that the ratio of subhalo mass to SubSub luminosity within r_t corresponds to the ratio between main halo mass and SubSm luminosity (from Fig. 3) within the scaled radius r_t/f, where $f = (V_{\rm max}/209\,{\rm km\,s^{-1}})$. We must also correct for the SubSub luminosity below the mass limit $M_{\rm min} = 10^5 f^3\ {\rm M}_\odot$, scaling down the resolution limit of our simulation appropriately for the subhalo. The SubSub luminosity must then be boosted by a factor $(M_{\rm min}/M_{\rm lim})^{0.226}$ where $M_{\rm lim}$ is the free-streaming mass, $10^{-6}\,{\rm M}_\odot$, in the example given above. For definiteness, we adopt $M_{\rm lim} = 10^{-6}\,{\rm M}_\odot$ in the discussion below, although none of our conclusions would change if we adopted, for example, $M_{\rm lim} = 10^{-12}\,{\rm M}_\odot$.

We now consider the expected appearance and detectability of these various components. The diffuse emission from the Milky Way's halo (MainSm) is distributed across the whole sky falling away smoothly from the Galactic centre. A randomly placed observer at $r = 8\,$kpc sees half the flux within 13 degrees of the Galactic centre, most of this well outside the Galactic plane where contamination is strongest. Assuming NFW structure for individual subhalos, half the diffuse emission from each object falls within the angular radius corresponding to $r_{\rm half} = 0.089\,r_{\rm max}$. Because of their large typical distances, these subhalos are almost uniformly

distributed across the sky. The luminosity from unresolved subhalos (MainUn) is similarly distributed and will appear smooth in γ-ray sky maps, with a centre to anticentre surface brightness contrast of only 1.54. Half the luminosity from (sub-)subhalos within an individual subhalo falls within an angular radius corresponding to $\sim 0.6\,r_t$; this is usually much more extended than the SubSm emission from the same subhalo.

This information allows us finally to calculate the relative detectability of the various components. As argued above, the signal-to-noise for detection by an optimal filter against a bright uniform background can be written as $S/N \propto F/\theta_h$, where F is the total flux, θ_h is the angle containing half this flux and the constant of proportionality depends weakly on profile shape but strongly on the particle-physics and observational parameters (the factor $\mathscr{G}$ above). To account for the finite angular resolution of the observation, we replace θ_h with $\theta_h' = (\theta_h^2 + \theta_{\rm psf}^2)^{1/2}$. For example, $\theta_{\rm psf} \simeq 10\,$arcmin is the characteristic angular resolution of the LAT detector of the recently launched GLAST telescope at the relevant energies[19]. In reality, the background at these energies is not uniform and is relatively poorly known[20,21]. In the Supplementary Information, we show that this is likely to reduce the detectability of the main smooth halo relative to that of subhalos by a factor up to ten compared to the numbers we quote below which are based on the simple assumption of a uniform background.

In Fig. 4 we combine data for 1000 randomly placed observers at $r = 8\,$kpc. Panel (a) shows histograms of the S/N for detecting SubSm and SubSub emission from the 30 highest S/N subhalos, and also shows the expected S/N for known satellites of the Milky Way. These are all expressed in units of the S/N for detecting the MainSm emission. Three important conclusions follow immediately: (1) no subhalo is expected to have S/N more than $\sim 10\%$ that of the main halo even accounting for the expected effects of the non-uniform background; (2) the most easily detectable dark subhalo is predicted to have 5 times larger S/N than the

LMC; and (3) the S/N predicted for SubSub emission is always much lower than that predicted for SubSm emission because of the much greater angular extent of the former.

Panels (b) to (f) of Fig. 4 show histograms of the masses, $V_{\rm max}$ values, distances, angular half-light radii, and fluxes (relative to the flux from the main halo) of the 30 highest S/N subhalos. These are compared with the distributions for the known satellites of the Milky Way where appropriate. For the fluxes and half-light radii we show separate histograms for the SubSm and SubSub emission. A second set of important conclusions follow. If subhalos are detected, then the highest S/N systems: (4) will typically have masses and circular velocities well below those inferred for the currently known satellites of the Milky Way; (5) will have angular half-light radii below 10 arcmin and so will not be resolved by GLAST; (6) will be at distances ~ 4 kpc; and (7) will typically have SubSm and SubSub fluxes which are factors of 10^{-4} and 10^{-6} times lower than those of the main halo, respectively.

These conclusions differ substantially from earlier work. Very small-scale substructure (below the resolution limit of our simulations) does not affect the detectability of dark matter annihilation in the Milky Way's halo. This is true both for the smooth main halo (contradicting references 4, 5 and 22 amongst others) and for its subhalos (contradicting 6, 23 and 24). Emission should be much more easily detected from the main halo than from subhalos (contradicting 25 and 26, but in agreement with 27), even though the total flux is dominated by substructures (contradicting 28 and 29). The most easily detectable subhalo is expected to be a relatively nearby object of lower mass than any known Milky Way satellite (contradicting 23 and 25). Almost all of these differences stem from the differing spatial distribution of small-scale substructure and smooth dark matter which our simulations are able to trace reliably because of their high resolution.

The GLAST satellite is now in orbit and accumulating a γ-ray image of the whole sky. If Nature obeys supersymmetry and the parameters of the theory are favourable, in a few years we may have a direct image of the Galaxy's dark halo. If we are really lucky, we may also detect substructures both without and with stars. This would provide a convincing confirmation of the Cold Dark Matter theory.

References

1. Bertone, G., Hooper, D. & Silk, J. Particle dark matter: evidence, candidates and constraints. *Physics Reports* **405**, 279–390 (2005).
2. Gehrels, N. & Michelson, P. GLAST: the next-generation high energy gamma-ray astronomy mission. *Astroparticle Physics* **11**, 277–282 (1999).
3. Baltz, E. A. *et al.* Pre-launch estimates for GLAST sensitivity to dark matter annihilation signals. *Journal of Cosmology and Astro-Particle Physics* **7**, 013 (2008).
4. Calcáneo-Roldán, C. & Moore, B. Surface brightness of dark matter: Unique signatures of neutralino annihilation in the galactic halo. *Phys Rev D* **62**, 123005 (2000).
5. Berezinsky, V., Dokuchaev, V. & Eroshenko, Y. Small-scale clumps in the galactic halo and dark matter annihilation. *Phys Rev D* **68**, 103003 (2003).
6. Strigari, L. E., Koushiappas, S. M., Bullock, J. S. & Kaplinghat, M. Precise constraints on the dark matter content of MilkyWay dwarf galaxies for gamma-ray experiments. *Phys Rev D* **75**, 083526 (2007).
7. Berezinsky, V., Bottino, A. & Mignola, G. High energy gamma-radiation from the Galactic center due to neutralino annihilation. *Physics Letters B* **325**, 136–142 (1994).
8. Bergström, L., Ullio, P. & Buckley, J. H. Observability of gamma rays from dark matter neutralino annihilations in the Milky Way halo. *Astroparticle Physics* **9**, 137–162 (1998).
9. Navarro, J. F., Frenk, C. S. & White, S. D. M. A Universal Density Profile from Hierarchical Clustering. *Astrophys. J.* **490**, 493–508 (1997).
10. Strigari, L. E. *et al.* Redefining the Missing Satellites Problem. *Astrophys. J.* **669**, 676–683 (2007).
11. Peñarrubia, J., McConnachie, A. W. & Navarro, J. F. The Cold Dark Matter Halos of Local Group Dwarf Spheroidals. *Astrophys. J.* **672**, 904–913 (2008).
12. Springel, V. *et al.* The Aquarius Project: Cold dark matter under a numerical microscope. In *High Performance Computing in Science and Engineering, Munich 2007*, edited by S. Wagner, M. Steinmetz, A. Bode & M. Brehm, 93–108 (Springer, Berlin, 2008)

13. Diemand, J. *et al.* Clumps and streams in the local dark matter distribution. *Nature* **754**, 735–738 (2008).

14. Prada, F., Klypin, A., Flix, J., Martínez, M. & Simonneau, E. Dark Matter Annihilation in the Milky Way Galaxy: Effects of Baryonic Compression. *Physical Review Letters* **93**, 241301 (2004).

15. Mohayaee, R., Shandarin, S. & Silk, J. Dark matter caustics and the enhancement of self-annihilation flux. *Journal of Cosmology and Astro-Particle Physics* **5**, 015 (2007).

16. Hofmann, S., Schwarz, D. J. & Stöcker, H. Damping scales of neutralino cold dark matter. *Phys Rev D* **64**, 083507 (2001).

17. De Lucia, G. *et al.* Substructures in cold dark matter haloes. *Mon. Not. R. Astron. Soc.* **348**, 333–344 (2004).

18. Gao, L., White, S. D. M., Jenkins, A., Stoehr, F. & Springel, V. The subhalo populations of ΛCDM dark haloes. *Mon. Not. R. Astron. Soc.* **355**, 819–834 (2004).

19. Michelson, P. F. The Large Area Telescope. In Ritz, S., Michelson, P. & Meegan, C. A. (eds.) *The First GLAST Symposium*, vol. 921 of *American Institute of Physics Conference Series*, 8–12 (2007).

20. Hunter, S. D. *et al.* EGRET Observations of the Diffuse Gamma-Ray Emission from the Galactic Plane. *Astrophys. J.* **481**, 205–240 (1997).

21. Strong, A. W., Moskalenko, I. V. & Reimer, O. Diffuse Galactic Continuum Gamma Rays: A Model Compatible with EGRET Data and Cosmic-Ray Measurements. *Astrophys. J.* **613**, 962–976 (2004).

22. Aloisio, R., Blasi, P. & Olinto, A. V. Gamma-Ray Constraints on Neutralino Dark Matter Clumps in the Galactic Halo. *Astrophys. J.* **601**, 47–53 (2004).

23. Kuhlen, M., Diemand, J. & Madau, P. The Dark Matter Annihilation Signal from Galactic Substructure: Predictions for GLAST. *Astrophys. J., in press* (2008). `ArXiv:0805.4416`.

24. Strigari, L. E. *et al.* The Most Dark-Matter-dominated Galaxies: Predicted Gamma-Ray Signals from the Faintest Milky Way Dwarfs. *Astrophys. J.* **678**, 614–620 (2008).

25. Evans, N. W., Ferrer, F. & Sarkar, S. A travel guide to the dark matter annihilation signal. *Phys Rev D* **69**, 123501 (2004).

26. Koushiappas, S. M., Zentner, A. R. & Walker, T. P. Observability of gamma rays from neutralino annihilations in the Milky Way substructure. *Phys Rev D* **69**, 043501 (2004).

27. Stoehr, F., White, S. D. M., Springel, V., Tormen, G. & Yoshida, N. Dark matter annihilation in the halo of the Milky Way. *Mon. Not. R. Astron. Soc.* **345**, 1313–1322 (2003).

28. Peirani, S., Mohayaee, R. & de Freitas Pacheco, J. A. Indirect search for dark matter: Prospects for GLAST. *Phys Rev D* **70**, 043503 (2004).

29. Pieri, L., Branchini, E. & Hofmann, S. Difficulty of Detecting Minihalos via γ Rays from Dark Matter Annihilation. *Physical Review Letters* **95**, 211301 (2005).

30. Springel, V., White, S. D. M., Tormen, G. & Kauffmann, G. Populating a cluster of galaxies - I. Results at z=0. *Mon. Not. R. Astron. Soc.* **328**, 726–750 (2001).

Competing interests The authors declare that they have no competing financial interests.

Correspondence and requests for materials should be addressed to V.S. (email: vspringel@mpa-garching.mpg.de).

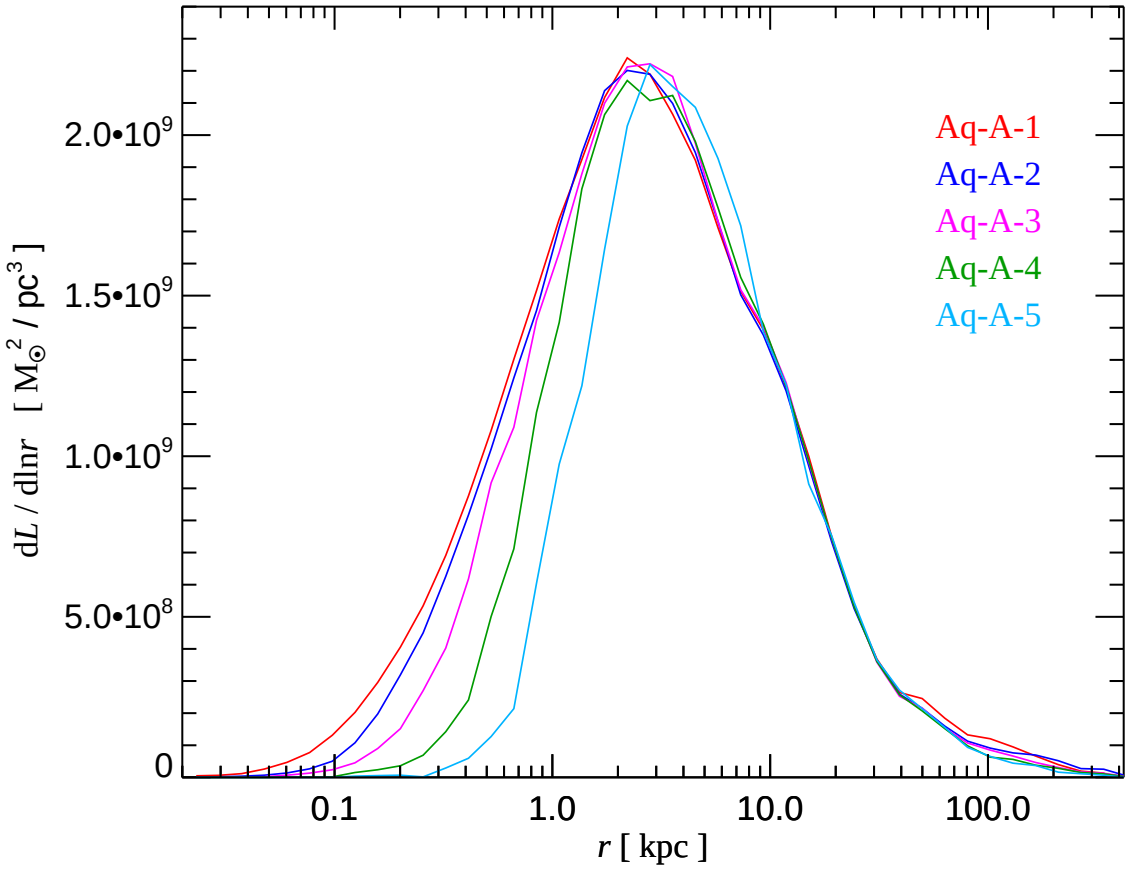

Figure 1: Annihilation luminosity as a function of radius for the diffuse dark matter component of Milky Way halos. These simulations assume $\mathscr{G} = 1$ and a Universe with mean matter density $\Omega_{\rm m} = 0.25$, cosmological constant density $\Omega_\Lambda = 0.75$, Hubble constant $H_0 = 73\,{\rm km\,s^{-1}Mpc^{-1}}$, primordial spectral index $n = 1$ and present fluctuation amplitude $\sigma_8 = 0.9$. In this representation, the total emitted luminosity is proportional to the area under each curve. The particle mass in the simulations is $1712\,{\rm M}_\odot$ for Aq-A-1, and grows to 1.37×10^4, 4.91×10^4, $3.93\times10^5\,{\rm M}_\odot$ and $3.14\times10^6\,{\rm M}_\odot$ for Aq-A-2, Aq-A-3, Aq-A-4 and Aq-A-5, respectively. The fluctuations at large radii are due to subhalos below our detection limit. These curves were calculated by estimating a density local to each N-body particle through a Voronoi tesselation of the full particle distribution and then summing the annihilation luminosities of individual particles in a set of logarithmically spaced spherical shells. Note that the vertical axis is linear, so these curves demonstrate numerical convergence at the percent level in the detailed structure of our main halo down to scales below 1 kpc.

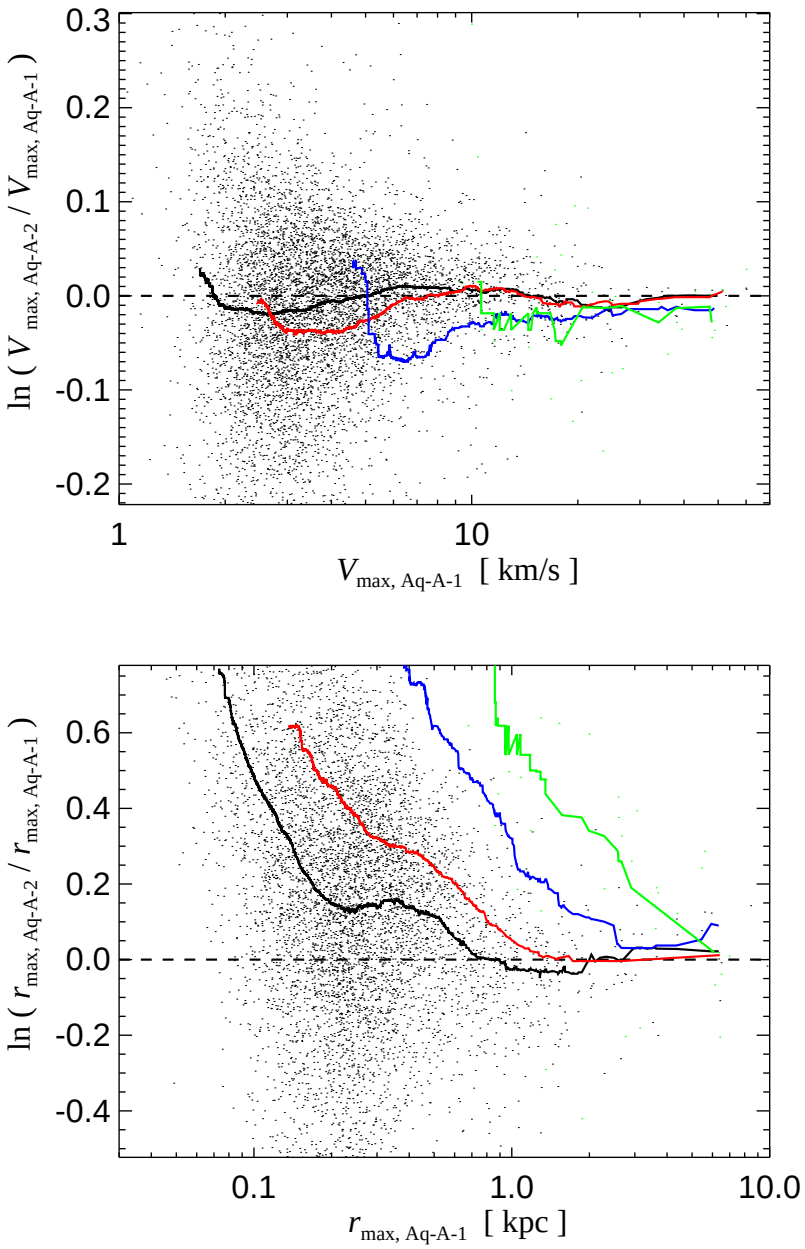

Figure 2: Structural properties of dark matter subhalos as a function of simulation resolution. *Upper panel*: $\ln(V_{\mathrm{max,Aq-A-2}}/V_{\mathrm{max,Aq-A-1}})$ against $V_{\mathrm{max,Aq-A-1}}$ for 6711 matched subhalos detected by the SUBFIND algorithm[30] within 433 kpc of halo centre in our two highest resolution simulations, Aq-A-1 and Aq-A-2. The radius 433 kpc encloses an overdensity 200 times the cosmic mean. The black solid line shows the running median of this distribution. Red, blue and green lines give similar median curves for matches of the lower resolution simulations to the highest resolution simulation, Aq-A-1. *Lower panel*: as above but for the ratio of characteristic sizes (r_{max}) as a function of that in the highest resolution simulation. We have checked that convergence in the subhalo mass is similarly good and that these results apply equally well to subhalos inside 50 kpc.

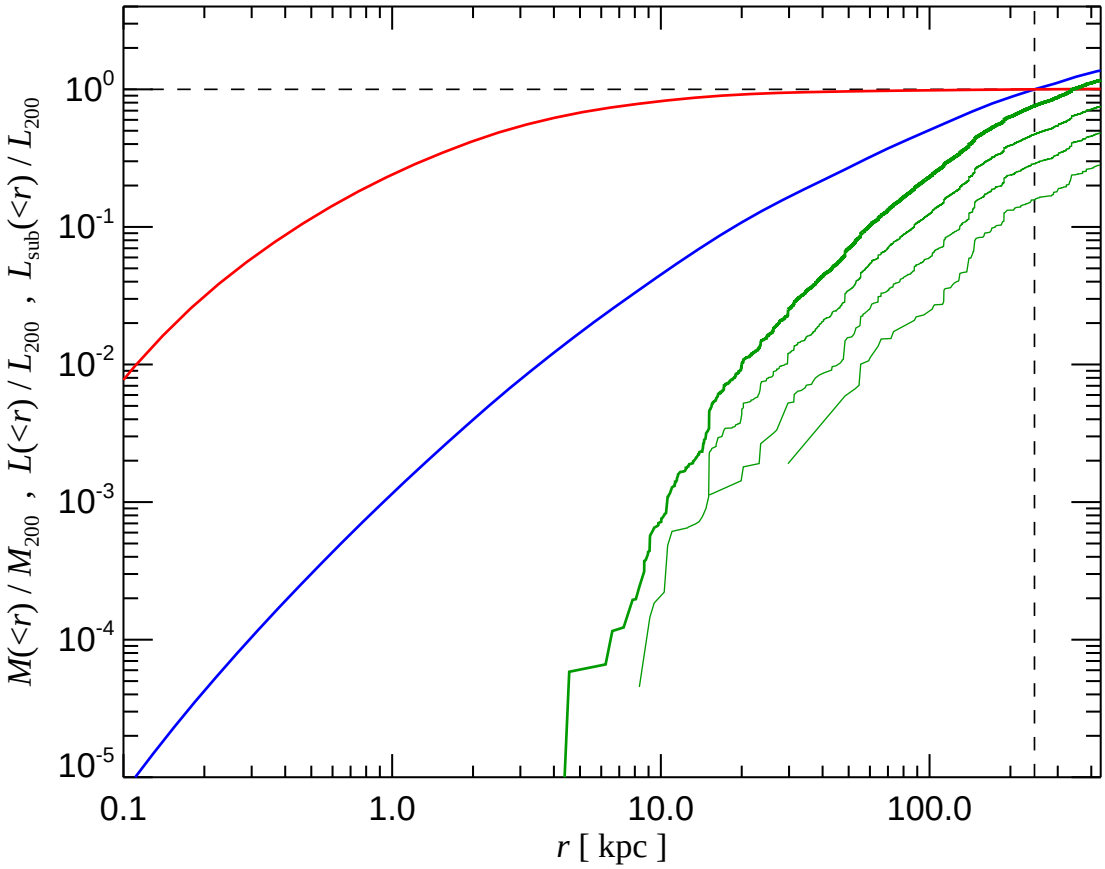

Figure 3: Radial dependence of the enclosed mass and annihilation luminosity of various halo components. The blue line gives enclosed dark matter mass in units of M_{200}, the value at r_{200} (the radius enclosing a mean density 200 times the critical value, marked in the plot by a vertical dashed line). The red line gives the luminosity of smooth main halo annihilation (MainSm) in units of L_{200}, its value at r_{200}. The green lines give the luminosity of smooth subhalo annihilation (SubSm) for various lower limits to the subhalo mass considered; the solid thick line is for $M_{\rm min} = 10^5\,{\rm M}_\odot$, the thin lines for $M_{\rm min} = 10^6, 10^7$ and $10^8\,{\rm M}_\odot$. Note that the shape of these lines is insensitive to $M_{\rm min}$, and that their normalization is proportional to $M_{\rm min}^{-0.226}$.

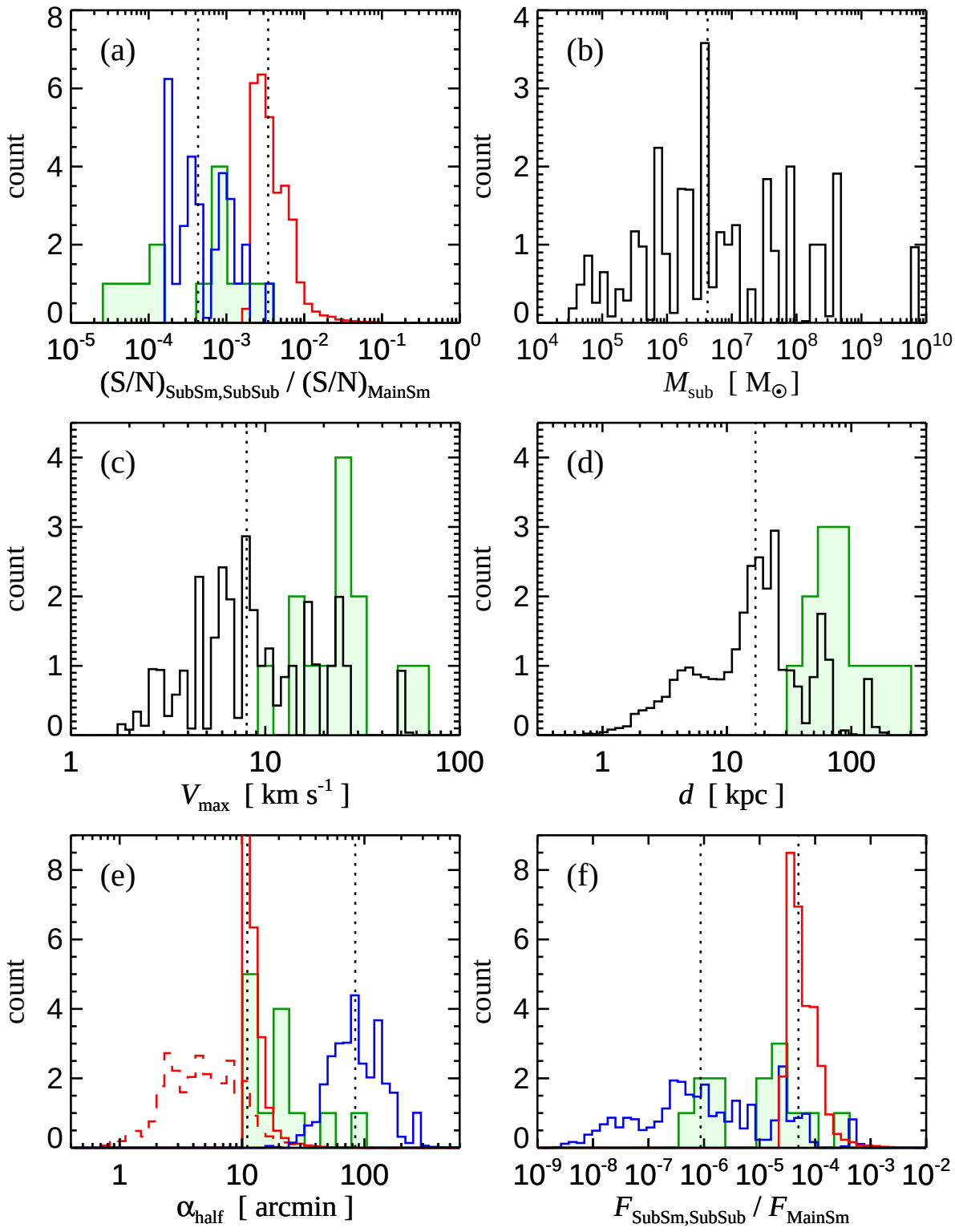
(a)
count
(S/N)SubSm,SubSub / (S/N)MainSm
(b)
count
Msub [M⊙]
(c)
count
Vmax [km s-1]
(d)
count
d [kpc]
(e)
count
αhalf [arcmin]
(f)
count
FSubSm,SubSub / FMainSm

Figure 4: Observability of subhalos. The histograms show the properties of the 30 highest S/N subhalos seen by each of 1000 observers placed at random 8 kpc from halo centre, assuming a 10 arcmin observational beam. The histograms are divided by 1000 so they sum to 30. Panel (a): the 30 highest S/N values for SubSm (red) and SubSub (blue) emission. These do not necessarily come from the same subhalos. The SubSub S/N values lie well below the SubSm values – subhalo detectability is not influenced by internal substructure. Panels (b), (c) and (d): histograms of the masses, $V_{\rm max}$ values and distances of the 30 halos with highest S/N SubSm emission. For these same halos panels (e) and (f) show half-light radii and fluxes separately for the SubSm (red) and the SubSub (blue) emission. In panel (e) the dashed and solid red histograms show values before and after convolution with the telescope beam. For subhalos with $V_{\rm max} < 5\,{\rm km\,s^{-1}}$ we have suppressed numerical noise by replacing the measured $r_{\rm max}$ by a value drawn from a suitably scaled version of the distribution measured at larger $V_{\rm max}$ for subhalos within 50 kpc. This substitution has a modest effect on the low mass tails of our distributions. Fluxes are expressed in units of the flux from the main halo. Dashed vertical lines mark median values. The single highest S/N subhalos detected by each of our 1000 "observers" are biased towards smaller and nearer objects; their median values are $(S/N)_{\rm SubSm} = 0.015\,(S/N)_{\rm MainSm}$, $V_{\rm max} = 6\,{\rm km\,s^{-1}}$, $M_{\rm sub} = 2\times10^6\,{\rm M_\odot}$ and $d = 4\,{\rm kpc}$. Light green histograms show the distributions predicted for SubSm emission from 13 known satellites of the Milky Way, based on published mass models[11].

Supplementary Information

V. Springel[1], S. D. M. White[1], C. S. Frenk[2], J. F. Navarro[3,4],
A. Jenkins[2], M. Vogelsberger[1], J. Wang[1], A. Ludlow[3], A. Helmi[5]

This document provides supplementary information for our Letter to Nature. In particular, we detail the signal-to-noise calculation and the treatment of the background.

Optimal filter for detection

The search for γ-ray photons from dark matter annihilation is made difficult by the low photon flux received here on Earth (or in orbit for that matter), which introduces the familiar limitations of Poisson statistics. In this case, the discrimination against the background flux and other sources of noise can benefit from an optimal filter for detection.

For definiteness, let $n_\gamma(\theta,\phi)$ describe the mean specific intensity of γ-ray photons from dark matter annihilation on the sky (i.e. photons per second, per unit area, and unit solid angle). Further, let $b_\gamma(\theta,\phi)$ be the specific intensity of background photons. We define as expected signal the quantity

$$\langle S\rangle = \tau A_{\rm eff}\int w(\theta,\phi)\, n_\gamma(\theta,\phi){\rm d}\Omega, \qquad (1)$$

where $w(\theta,\phi)$ is a suitable *filter* function, τ is the observational integration time, and $A_{\rm eff}$ is the effective area of the telescope. Likewise, the total expected photon count within the same filter function is

$$\langle T\rangle = \tau A_{\rm eff}\int w(\theta,\phi)\,[n_\gamma(\theta,\phi)+b_\gamma(\theta,\phi)]{\rm d}\Omega. \qquad (2)$$

To establish the significance of the signal, we need to compare its expectation value to the dispersion of the total photon count. We define as *signal-to-noise* ratio the quantity

$$(S/N) = \langle S\rangle \,/\, \left[\left\langle T^2\right\rangle - \langle T\rangle^2\right]^{1/2}. \qquad (3)$$

Since the arriving photons sample the signal and the background distribution as a Poisson process, we have

$$(S/N)^2 = \tau A_{\rm eff}\frac{[\int w(\theta,\phi)\, n_\gamma(\theta,\phi){\rm d}\Omega]^2}{\int w^2(\theta,\phi)\,[n_\gamma(\theta,\phi)+b_\gamma(\theta,\phi)]{\rm d}\Omega}. \qquad (4)$$

It is easy to show that the signal-to-noise is maximized if the filter w is chosen as

$$w(\theta,\phi) \propto \frac{n_\gamma(\theta,\phi)}{n_\gamma(\theta,\phi)+b_\gamma(\theta,\phi)}. \qquad (5)$$

For this *optimal filter*, the resulting signal-to-noise is then given by

$$S/N = \sqrt{\tau A_{\rm eff}}\left[\int \frac{n_\gamma^2(\theta,\phi)}{n_\gamma(\theta,\phi)+b_\gamma(\theta,\phi)}{\rm d}\Omega\right]^{1/2}. \qquad (6)$$

Note that *if the background dominates* (the regime relevant for dark matter annihilation in the Milky Way, except perhaps in the very centers of halos and subhalos), n_γ can be neglected against b_γ in the denominator above, and the optimal filter shape is simply proportional to the signal profile divided by the background profile. If the variation of the background over the source can be neglected, the optimal filter is just given by the signal shape. Another important consequence of background dominance is that the overall amplitude of the background drops out when the signal-to-noise of two different dark matter structures in the Milky Way is compared.

Signal-to-noise calculation for different flux components

We now calculate the optimal S/N for the different components in our Milky Way simulation model. To account for the finite angular resolution of the telescope (of order $\theta_{\rm psf}\sim$

[1]Max-Planck-Institute for Astrophysics, Karl-Schwarzschild-Str. 1, 85740 Garching, Germany
[2]Institute for Computational Cosmology, Dep. of Physics, Univ. of Durham, South Road, Durham DH1 3LE, UK
[3]Dep. of Physics & Astron., University of Victoria, Victoria, BC, V8P 5C2, Canada
[4]Dep. of Astron., University of Massachusetts, Amherst, MA 01003-9305, USA
[5]Kapteyn Astronomical Institute, Univ. of Groningen, P.O. Box 800, 9700 AV Groningen, The Netherlands

10 arcmin for GLAST at the relevant energies), we convolve the raw infinite-resolution signal n_γ with a Gaussian point-spread-function (PSF),

$$w_{\rm psf}(\vec{\alpha}) = \frac{\ln 2}{\pi\theta_{\rm psf}^2}\exp\left(-\ln 2\frac{\vec{\alpha}^2}{\theta_{\rm psf}^2}\right), \qquad (7)$$

before using it to calculate the S/N with equation (6). We have here chosen to parameterize the PSF with the angle $\theta_{\rm psf}$ that contains half the light, for consistency with the half-light angles we use to characterize the sources. (The angle that contains 68% of the light is larger than $\theta_{\rm psf}$ by a factor 1.28.) Note that smoothing allows us to continue to use the assumption of background dominance even for cuspy dark matter halos, which in the infinite resolution case can have a diverging surface brightness in their centre.

Component "SubSm", resolved subhalos

We assume that the background does not vary significantly over the angular extent of a subhalo at location $\vec{\alpha}$. It is then numerically straightforward first to calculate the specific intensity of a given subhalo on the sky (characterized by its total luminosity, distance, and half-light angle), then to convolve it with the Gaussian PSF, and finally to calculate its S/N with equation (6). The result can be written as

$$(S/N)_{\rm SubSm} = f_{\rm SubSm}\left(\theta_h/\theta_{\rm psf}\right)\left[\frac{\tau A_{\rm eff}}{b_\gamma(\vec{\alpha})}\right]^{1/2}\frac{F}{(\theta_h^2+\theta_{\rm psf}^2)^{1/2}}, \qquad (8)$$

where $F = L/(4\pi d^2)$ is the photon flux of the source, and $f_{\rm SubSm}(x)$ is a factor of order unity which depends on the detailed shape of the source. As the shape varies depending on whether the source is resolved or not, $f_{\rm SubSm}$ is a function of the ratio $x = \theta_h/\theta_{\rm psf}$ of the half-light angle and the angular resolution. In the top panel of Figure 5, we show $f_{\rm SubSm}$ for projected NFW halos, our adopted model for the SubSm emission. For a source that is completely unresolved, $\theta_h \ll \theta_{\rm psf}$, the factor $f_{\rm SubSm}$ approaches $\sqrt{(\ln 2)/2\pi} \simeq 0.332$, the value expected for a Gaussian signal. Note however that the overall variation of $f_{\rm SubSm}$ between unresolved and well resolved subhalos is very modest, and at most a factor ~ 2.

Component "SubSub", substructures in subhalos

As we have shown in this Letter, the radial distribution of substructure is strongly antibiased with respect to the mass of the parent halo. This in turn applies to (sub-)substructure within a subhalo. An immediate consequence is that the surface brightness profile of (sub-)substructure is much more extended than that of the parent subhalo, and unlike that of the parent halo it is strongly affected by tidal truncation and the associated mass loss in the outer parts of the halo.

We illustrate this qualitatively very different behaviour in Figure 6, which shows the azimuthally averaged surface brightness profile we adopt for typical $V_{\rm max} = 10\,{\rm km\,s^{-1}}$ subhalos at various distances from the Galactic centre and so with different tidal radii r_t. Each profile is split into the contribution from smooth DM (SubSm) and from (sub-)substructures (SubSub). Interestingly, the substructure surface brightness is nearly constant in projection. This remains the case when the halo is sharply tidally truncated at progressively smaller radii. The tidal truncation results in the loss of substructures so that the total SubSub luminosity declines strongly, yet the shape of the luminosity profile remains remarkably flat and can be approximated as a disk on the sky that becomes progressively fainter and smaller. In contrast, the total SubSm luminosity is little affected by tidal truncation and the main systematic effect with Galacto-centric distance is that subhalos of given mass become more concentrated with decreasing Galacto-centric distance, thus enhancing their SubSm luminosity.

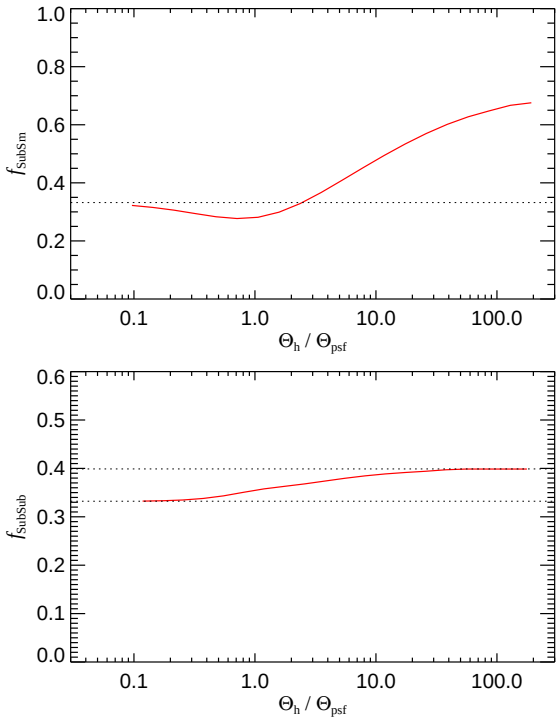

Figure 5: Signal-to-noise prefactors as a function of angular resolution. The top panel gives the prefactor for a subhalo with NFW profile seen in projection, while the bottom panel gives the prefactor for its much more extended (sub-)substructure emission.

For the purposes of calculating the signal-to-noise of the SubSub component, we assume that its surface brightness profile can be modelled as a uniform disk, subject to the smoothing of the finite angular resolution of the telescope. Again, we can

write the resulting signal-to-noise in the generic form

$$(S/N)_{\rm SubSub} = f_{\rm SubSub}\,(\theta_h/\theta_{\rm psf})\left[\frac{\tau A_{\rm eff}}{b_\gamma(\vec{\alpha})}\right]^{1/2}\frac{F}{(\theta_h^2+\theta_{\rm psf}^2)^{1/2}}\,, \tag{9}$$

where $F = L/(4\pi d^2)$ is the photon flux of the component, and θ_h is its half-light radius. In the bottom panel of Figure 5, we show the variation of $f_{\rm SubSub}$ with angular resolution. The factor $f_{\rm SubSub}$ varies smoothly between the value $\sqrt{(\ln 2)/2\pi} \simeq 0.332$ expected for an unresolved source, to the value $1/\sqrt{2\pi} \simeq 0.399$ expected for a well resolved disk-like component.

Component "MainSm", smooth main halo

The main halo's half-light angle of 13 degrees for the diffuse emission is resolved well with GLAST, but as our simulated emission maps have in principle higher resolution, we also smooth them with the PSF before calculating the S/N, for consistency. For definiteness we also average the main halo's diffuse emission in angular rings around the Galactic centre, and for 25 random observer positions. We note however that the dispersion arising from different observer viewpoints and orientations of the galactic plane assumed within the simulated halo is quite small.

A problematic point for the detection of the diffuse emission is the strong and variable background from other Galactic γ-ray emission, resulting mostly from the interaction of cosmic rays with the interstellar gas and from inverse Compton upscattering by electrons. A considerable body of literature is concerned with modelling the background and explaining the spectra observed with EGRET, in particular. The best predictions for the Galactic diffuse γ-ray background are obtained with complex codes like GALPROP [31], which treat CR interactions and propagation in the Galaxy in detail. However, the modelling uncertainties are still substantial, so we consider a few limiting cases for the spatial variation of the background.

First, let us examine the constant background case. Then the S/N of the MainSm component can be written as

$$(S/N)_{\rm MainSm} = f_{\rm MainSm}\left[\frac{\tau A_{\rm eff}}{b_\gamma}\right]^{1/2}\frac{F}{\theta_h}\,, \tag{10}$$

where we find $f_{\rm MainSm} \simeq 0.498$ from our simulation.

For a variable background, we consider three models, a simple analytic parameterization given by [8], of the form

$$b_\gamma(l,b) = 0.5 + \begin{cases} \dfrac{85.5}{\sqrt{[1+(\frac{l}{35})^2][1+(\frac{b}{1.1+0.022|l|})^2]}} & \text{for } |l| \geq 30^{\rm o} \\ \dfrac{85.5}{\sqrt{[1+(\frac{l}{35})^2][1+(\frac{b}{1.8})^2]}} & \text{for } |l| < 30^{\rm o} \end{cases} \tag{11}$$

where $-180^{\rm o} < l \leq 180^{\rm o}$ and $-90^{\rm o} < b \leq 90^{\rm o}$ are Galactic coordinates, and two γ-ray maps for the background calculated with the GALPROP code for propagation and interaction of cosmic rays in the Galaxy. The two GALPROP maps are the 'conventional' and 'optimized' models for Galactic γ-ray emission, as described by Strong et al. [31]. We show all-sky maps of these three background models in Figure 7.

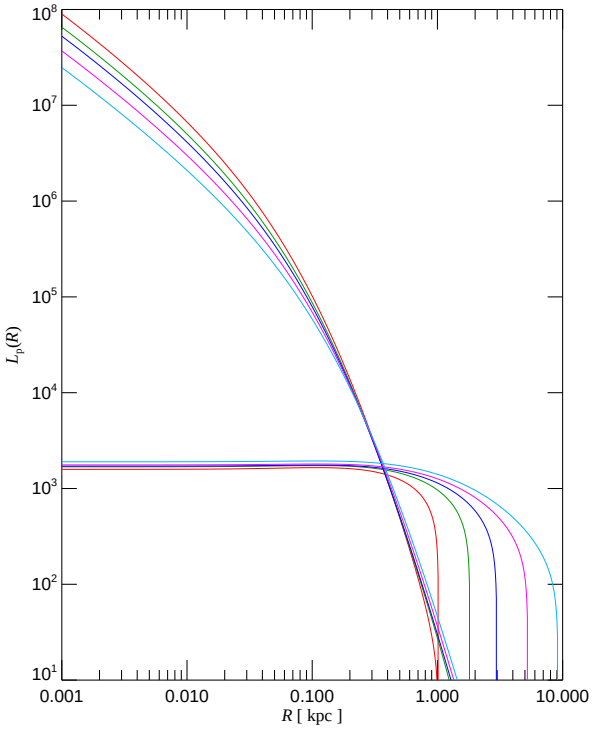

Figure 6: Comparison of the shape of the surface brightness profile of typical subhalos with $V_{\rm max} = 10\,{\rm km\,s^{-1}}$ at different Galacto-centric distances equal to $d = 400$, 200, 50 and 12.5 kpc from the halo center, as seen by a distant observer. The upper set of solid lines shows the surface brightness profile of the subhalo's diffuse emission (component SubSm), which we model as a NFW profile that is truncated at the tidal truncation radius. The lower set of solid lines gives the surface brightness profile of all (sub-)substructure emission (component SubSub) in the subhalo, extrapolated down to $10^{-6}\,{\rm M}_\odot$, while the dotted lines show the total profile. Note that the central surface brightness of the smooth emission as well as its total luminosity actually increase nearer to the centre of the main halo, because subhalos of equal $V_{\rm max}$ are on average more concentrated at smaller distances. On the other hand, the (sub-)substructure emission has a very different, nearly flat surface brightness profile, because most substructures are located in the outer parts of the subhalo. As a result, tidal truncation strongly reduces the luminosity of this component and leads to a decline of the SubSub surface brightness for smaller distances.

The optimal filter will automatically down-weight the signal where the background is high, so in principle the S/N can be directly calculated with these background maps over the whole sky. For this perhaps optimistic approach, we can again write

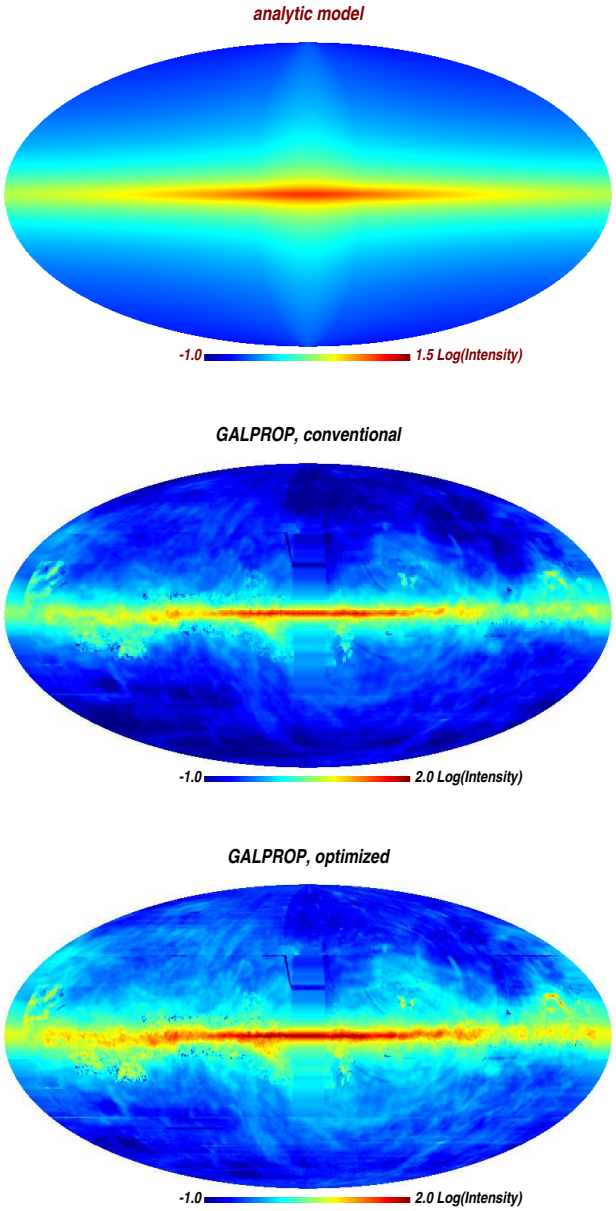

Figure 7: Models for the diffuse γ-ray background of the Milky Way. The top panel shows an all-sky map of a simple analytic background model given in [8], while the middle and bottom panels show background models both for the 'conventional' and 'optimized' GALPROP models of ref. [31], where the optimized model has been tuned to approximately reproduce the observed EGRET spectrum. For the maps, the analytic model and the conventional GALPROP model have been normalized to their mean background over the whole sky. The optimized model is normalized to the mean value of the conventional model, to illustrate its slightly elevated overall background level.

the S/N as

$$(S/N)_{\rm MainSm} = f_{\rm MainSm}\left[\frac{\tau A_{\rm eff}}{\langle b_\gamma\rangle}\right]^{1/2}\frac{F}{\theta_h}, \qquad (12)$$

where now $\langle b_\gamma\rangle$ is the background averaged over the whole sky. We obtain $f_{\rm MainSm} = 0.183$ for the background model of equation (11), $f_{\rm MainSm} = 0.205$ for the conventional GALPROP map, and $f_{\rm MainSm} = 0.198$ for the optimized GALPROP map. The differences between the background models are hence quite small, and the S/N coefficient reduces approximately by a factor $\sim 2.5-2.8$ compared with the more favorable constant background. If the background is averaged only over the high latitude sky (say for $b > 10^{\rm o}$) to account for the fact that most subhalos reside there, the S/N prefactor reduces further by a factor 1.3 for the analytic model, and by 1.6 for the GALPROP maps.

Note that the S/N of subhalos will in general also change for a variable background, depending on their position; the majority will slightly increase their relative S/N as they are located at positions where the background lies below the sky-averaged background, while for the others the relative S/N will decrease. This effectively broadens the S/N distribution of subhalos relative to the S/N of the main halo.

However, the above approach of integrating over the whole sky is probably too optimistic in reality, as the background is not known very accurately close to the Galactic center and close to the disk. A more conservative approach may therefore be to cut out this region entirely, for example by excluding the region 5 degrees above and below the Galactic plane. This $|b| < 5^{\rm o}$ cut disregards a bit less than 10% of the sky, but since the main halo's emission is highly concentrated towards the centre, the impact on the S/N will be larger. We find that the coefficient $f_{\rm MainSm}$ drops by a factor 2.04 in this case when the analytic background model given in equation (11) is used. If the cut is enlarged to exclude $|b| < 10^{\rm o}$ instead, the drop is instead a factor of 3.00. For the GALPROP models, the corresponding changes are slightly smaller; for the $|b| < 5^{\rm o}$ cut, they evaluate to factors of 1.53 and 1.44 for the conventional and optimized models, respectively, while for the $|b| < 10^{\rm o}$ cut the numbers are 2.21 and 2.10, respectively.

Component "MainUn", unresolved subhalos

As we have seen in the Letter, an extrapolation of the simulated substructure mass spectrum down to $10^{-6}\,{\rm M}_\odot$ suggests that the cumulative luminosity of all substructures in fact dominates the total emission of the Milky Way as seen by a distant observer, being larger by a factor ~ 232 than the main halo's diffuse luminosity within a radius of 246 kpc. However, most of these substructures are much further from the Sun than the Galactic centre, so the total substructure flux received on Earth is only a factor 1.9 larger than that from the smooth main halo.

We expect this total substructure flux to be nearly uniformly distributed over the sky, which will make it hard to detect in practice. To obtain a model for this distribution, we first construct a map of the flux of all resolved substructures, each of

them represented by the sum of their SubSm and SubSub luminosities, the latter estimated as described in the Letter. In total, the SubSub luminosity assigned to the subhalos corresponds to 4.9 times the total SubSm luminosity, most of it in objects at $R > 20\,\mathrm{kpc}$. We then still miss the luminosity from independent subhalos below our mass resolution limit, as well as from their (sub-)substructure, which is the component MainUn. Based on our extrapolation of the total substructure luminosity within r_{200} as a function of mass resolution, we know that this raises the total luminosity contributed by substructures (SubSm + SubSub + MainUn) to 232 times the main halo's luminosity (MainSm), with a radial luminosity distribution that is self-similar to that of all resolved subhalos.

If we assume that the halo is spherically symmetric, we can use an analytic fit to the radial luminosity distribution of resolved substructures to calculate the surface brightness of the MainUn component over the sky. We then find that it contributes 85.7 times as much flux in total as the resolved subhalos and their (sub-)substructures (SubSm+SubSub), and nearly 1.9 times as much flux as the main halo (MainSm), but it has a maximum contrast of only 1.54 between Galactic center and anticenter. We caution however that small distortions in the halo shape in its outer parts could easily overwhelm this small contrast, so that one should not expect this gradient to be detectable in practice. In fact it is probably not even guaranteed that the center will be the brightest direction. Another plausible model for distributing the MainUn component is to assume that it is strictly proportional to the sum of the SubSm and SubSub components, but very heavily smoothed due to the huge number of unresolved substructures. For a smoothing of 30 degrees, the contrast between Galactic center and anticenter varies with observer position and is typically a factor 1.3 - 2.0, but there are fluctuations in other parts of the sky that are of similar amplitude.

In practice, it will be impossible to separate the MainUn component from DM annhihilation in more distant objects. We therefore exclude this component from our analysis in the Letter (see also below).

Ratios of S/N for different components

As is evident from the above expressions, the observation time and telescope aperture always drop out in ratios of different S/N values. Likewise, these ratios are invariant under a multiplicative factor for the background over the whole sky, provided the background stays sufficiently large that it dominates everywhere. Also, to the extent that the spectrum of the background is independent of direction, the spectral energy distribution of the annihilation radiation is unimportant for S/N ratios. Our analysis in the Letter is based on these simplifying assumptions, which allow quite general, and, we believe, robust statements about the relative detectability of different dark matter components in the Milky Way.

Note again that the near constancy of component MainUn over the sky will make it very difficult to tell it apart from the truly extragalactic background (both from annihilating dark matter and from other sources such as AGN), which has a level that is unknown. The component MainUn would have to be distinguished from the extragalactic background by a characteristic spectral signature or by its weak gradient across the sky. The former is (particle physics) model-dependent, while the latter will be difficult unless the Galactic component is dominant. For this reason, we consider that the main halo smooth component, with its strong gradient and higher mean surface brightness, is more likely to be detectable even if its total flux is somewhat lower.

For illustration, Figure 8 shows all-sky maps of the surface brightness distributions of the different emission components of the dark matter annihilation signals considered above. The top left panel gives the azimuthally averaged main halo's diffuse emission. In the top right panel, the total emission from resolved subhalos is shown. For simplicity and better visibility in the reproduction of the map, we represent each subhalo as a point source that is smoothed with a Gaussian beam of 40 arcmin, assigning to them the sum of the corresponding SubSm and SubSub emission. In the bottom left, we show the rather smooth emission of the component MainUn, assuming a spherical halo. Finally, the bottom right panel gives the sum of all components.

Uncertainties

Systematic and random errors

Our analysis of the signal-to-noise ratios assumed an accurate knowledge of the background level, so that it is only affected by random errors, in which case our simple treatment is appropriate. However, in reality background estimates have a substantial systematic uncertainty, which is perhaps as large as the difference between the 'conventional' and 'optimized' GALPROP models. This introduces systematic uncertainties that require an elaborate statistical analysis based on a multi-dimensional maximum likelihood treatment. This is clearly beyond the scope of the present study, but will certainly become part of the data analysis of the GLAST satellite (see also [3]).

Known versus unknown locations

For simplicity, we have also neglected in our analysis the differences in the required effective detection threshold between sources at known and unknown locations. The small dark matter substructures with the highest S/N for detection should correspond to truly dark subhalos without any stars; hence their location is initially unknown. As there are of order 5×10^5 resolution elements of $(10\,\mathrm{arcmin})^2$ on the sky, one would expect about 640 fluctuations above 3σ just from Gaussian statistics. One therefore has to detect a dark subhalo at unknown location at least with 5σ significance before it may qualify as a potential detection, while for a dwarf satellite at known location, as well as for the main halo, a less conservative threshold of 3σ may be assumed.

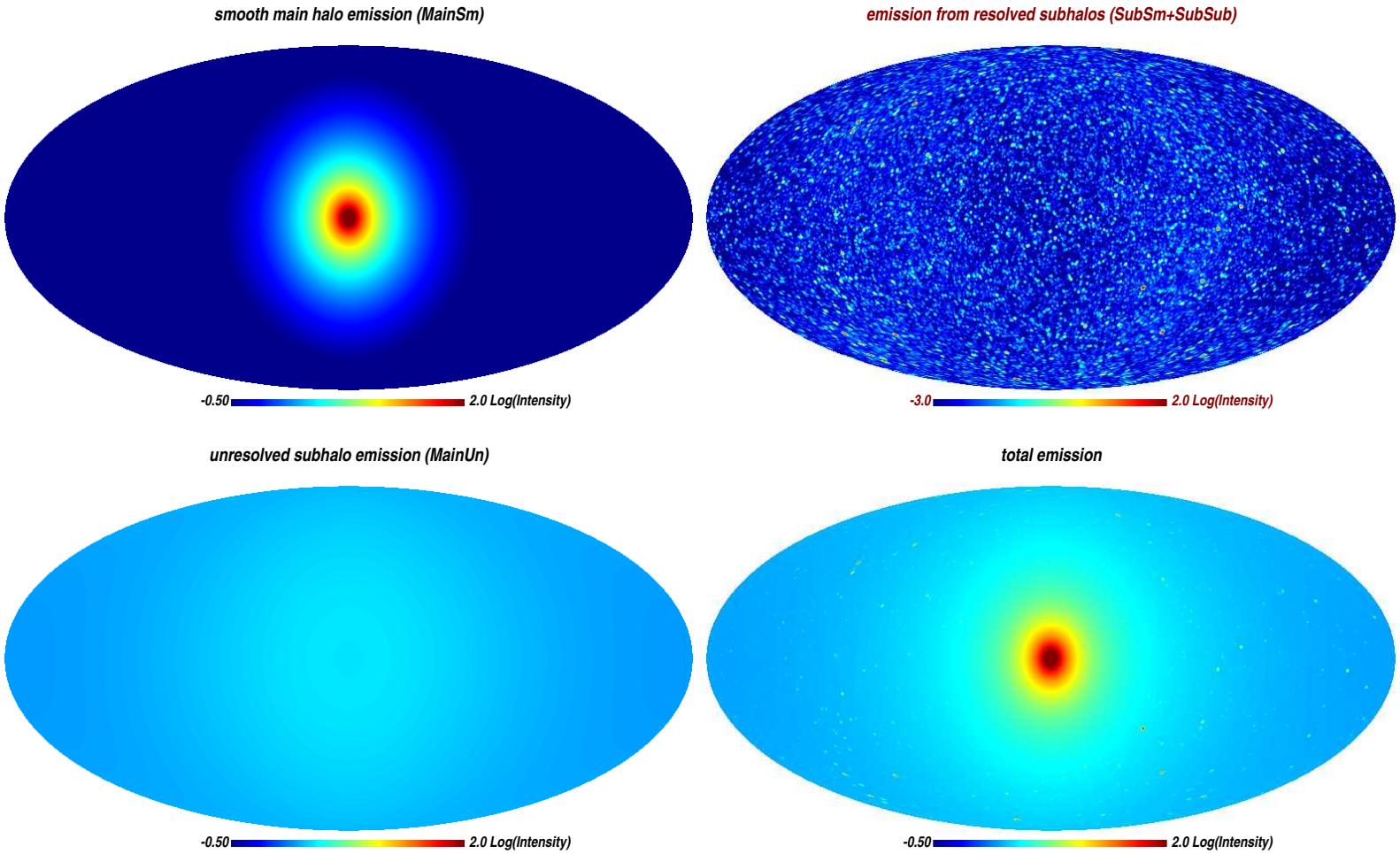

Figure 8: Different emission components. The top left panel shows an all-sky map of the main halo's diffuse emission (averaged for different observer positions and over azimuth), while the top right panel shows the emission from all resolved subhalos, from a random position on the Solar circle. The luminosities assigned to each subhalo include their contribution for all unresolved (sub-)substructure. For simplicity and for better graphical reproduction they have been represented as point sources that were smoothed with a Gaussian beam of 40 arcmin. The bottom left panel gives the expected surface brightness from all unresolved subhalos down to the free streaming limit, assuming a spherically symmetric halo. This is a very smooth component over the sky that dominates the total flux (its integrated flux is nearly 1.9 times the integrated flux from the main halo). Finally, the bottom right panel shows the total surface brightness from all components together. All maps show the surface brightness in units of the main halo's diffuse emission, and use the same mapping to color scale, except for the map of the resolved substructures, where the scale extends to considerably fainter surface brightness.

Effects of baryons

In our high-resolution simulations of a Milky Way like halo, we have neglected the effects of baryons on the growth of dark matter structures. While the dark matter dominance of the known dwarf satellites suggests that this approximation should be quite accurate for the dark matter subhalos, the central dark matter cusp of the main halo is likely modified by baryonic physics.

Most authors (but not all) argue that baryonic infall due to radiative cooling and disk formation leads to an adiabatic compression of the halo, which would enhance the smooth main halo emission relative to the other components we discuss, thus strengthening our conclusions. A comparably large variation comes from the scatter in concentration predicted among different realizations of halos of Milky Way mass [32]. The halo we analyze here is approximately a 1σ deviation towards high concentrations in the expected distribution, while the 'Via Lactea' simulations [13, 33] are 1-1.5σ deviations in the opposite sense. Since baryons are generically expected to increase halo concentration, it seems appropriate to analyze a halo that lies on the high side of the concentration distribution.

There have been suggestions in the literature that central dark matter cusps could perhaps be destroyed by dynamical processes such as stellar bars, supermassive black hole binaries, or rapid baryonic outflows from explosive feedback events. We note however that each of these scenarios for cusp removal is debated and discussed with conflicting numerical results in the literature, while the effect of adiabatic compression is found robustly in cosmological simulations with radiative cooling.

We also note that our conclusions do not rely on the dark matter distribution in the inner few degrees, where additional baryonic effects may play a role, for example a steepening of the dark matter cusp around the supermassive black hole at the Galactic centre [34, 35]. As we have shown above, the S/N for detection of the main halo drops only by a small factor if this uncertain region around the Galactic centre is excluded.

Energy dependence

An important problem in obtaining conclusive evidence for DM annihilation is to distinguish the signal from other astrophysical sources. For spatially resolved sources, the profile of the radiation on the sky can provide such a discrimination if it can be shown that the signal matches the theoretically expected dark matter distribution. This should be promising for the smoothly varying emission from the main halo of the Galaxy, especially if it is combined with the spectral information obtained from the energy distribution of the detected photons. The expected spectral shape of the radiation from dark matter annihilation has a characteristic form with a sharp cut-off near the mass of the dark matter particle, which is difficult to arrange with other astrophysical sources. Also, the peak of the annihilation spectrum typically lies at considerable higher energy in most SUSY models than the peak in the Galactic diffuse γ-ray background, which should further help in the discrimination.

If dark matter substructures are detected by GLAST, we expect them to be poorly resolved at best, so that their surface brightness profile will be of little help to identify them as a dark matter signal. Here the background uncertainty is less of a concern, but the signal must be distinguished from other astrophysical (point) sources. Again, a multiwavelength approach and the exploitation of spectral features [36, 37, 38] of the DM annihilation appears as a highly promising way to convincingly identify the origin of the signal.

References

31. Strong, A. W., Moskalenko, I. V. & Reimer, O. Diffuse Galactic Continuum Gamma Rays: A Model Compatible with EGRET Data and Cosmic-Ray Measurements. *Astrophys. J.* **613**, 962–976 (2004).

32. Neto, A. F. *et al*. The statistics of Λ CDM halo concentrations. *Mon. Not. R. Astron. Soc.* **381**, 1450–1462 (2007).

33. Diemand, J., Kuhlen, M. & Madau, P. Dark Matter Substructure and Gamma-Ray Annihilation in the Milky Way Halo. *Astrophys. J.* **657**, 262–270 (2007).

34. Gondolo, P. & Silk, J. Dark Matter Annihilation at the Galactic Center. *Physical Review Letters* **83**, 1719–1722 (1999).

35. Merritt, D., Milosavljević, M., Verde, L. & Jimenez, R. Dark Matter Spikes and Annihilation Radiation from the Galactic Center. *Physical Review Letters* **88**, 191301 (2002).

36. Baltz, E. A., Taylor, J. E. & Wai, L. L. Can Astrophysical Gamma-Ray Sources Mimic Dark Matter Annihilation in Galactic Satellites? *Astrophys. J. Let.* **659**, L125–L128 (2007).

37. Colafrancesco, S., Profumo, S. & Ullio, P. Detecting dark matter WIMPs in the Draco dwarf: A multiwavelength perspective. *Phys Rev D* **75**, 023513 (2007).

38. Dodelson, S., Hooper, D. & Serpico, P. D. Extracting the gamma ray signal from dark matter annihilation in the galactic center region. *Phys Rev D* **77**, 063512 (2008).